PCCP

PAPER

View Article Online
View Journal | View Issue

Cite this: *Phys. Chem. Chem. Phys.*, 2015, **17**, 19424

Influence of relative humidity on heterogeneous kinetics of NO_2 on kaolin and hematite†

Yongchun Liu, Chong Han, Jinzhu Ma, Xiaolei Bao and Hong He*

Received 16th April 2015,
Accepted 10th June 2015

DOI: 10.1039/c5cp02223a

www.rsc.org/pccp

In order to obtain reliable kinetic parameters, it is required to measure the reaction kinetics of important heterogeneous reactions at ambient relative humidity (RH). In this study, the uptake coefficients and HONO yields for the heterogeneous reaction of NO_2 on kaolin and hematite were measured at RH from 7% to 74% and at ambient pressure in the dark using a coated-wall flow tube reactor. The initial true uptake coefficient ($\gamma_{t,ini}$) of NO_2 at RH 7% was measured to be $(1.44 \pm 0.10) \times 10^{-7}$ and $(1.58 \pm 0.13) \times 10^{-6}$ on kaolin and hematite, respectively, while it decreased notably on both minerals, accompanied by an increase of HONO yields, as RH increased. The average $\gamma_{t,ini}$ at 32–74% RH was $(4.42 \pm 1.17) \times 10^{-8}$ and $(2.83 \pm 0.84) \times 10^{-7}$ on kaolin and hematite, respectively. The corresponding mean HONO yield was (36.0 ± 16.1)% and (75.9 ± 3.32)%, respectively.

Introduction

In the past few decades, due to their possible roles in atmospheric chemistry, considerable attention has been paid to heterogeneous reactions between nitrogen oxides (NO_x) and atmospheric particulate matter (APM), including soot,[1–4] mineral dust[5–8] and sea salt.[9,10] For example, heterogeneous reactions of NO_x on soot and mineral dust can produce gaseous HONO,[3,4,11] which is a daytime source of OH radicals;[12] while reactions between NO_x and sea salt might be a source of Cl radicals.[10] Mineral dust is an important component of APM, with a loading of 1000–3000 Tg per year.[13] Model results indicate that interactions of N_2O_5, O_3 and HO_2 radicals with dust can affect the photochemical oxidation cycle, causing a decrease of O_3 of up to 10% in and near to dust source areas.[13] The presence of dust could also result in a decrease in concentrations of SO_2, NO_y ($NO_3 + N_2O_3 + HNO_3$), and H_xO_y ($OH + HO_2 + H_2O_2$) by 10.3–52.5%, 16.0–99.7%, and 11.3–59.4%, respectively, through heterogeneous reactions under typical dust storm conditions.[14] In addition, it has been found that heterogeneous chemistry, including that of SO_2 and NO_x on dust, plays a significant role in regional haze formation in China.[15–17]

The uptake coefficient (γ) is one of the key parameters in modelling studies. Several studies have measured the γ of NO_2 on dust from Saharan or Asian source regions[5,18] and surrogate materials including $CaCO_3$,[7] Al_2O_3, Fe_2O_3, CaO, MgO, TiO_2[5,19] and clay minerals.[6] The γ of NO_2 on these samples varies from 10^{-4} to 10^{-9} depending on the substrates and experimental conditions,[20] and was recommended to be 1.2×10^{-8} by Crowley *et al.*[21] Except for a few reaction systems, such as reactions of NO_2 on TiO_2,[18,22,23] Saharan sand,[23] and $CaCO_3$,[7] however, most of these γ values were measured under dry conditions due to the limitations of the low pressure reactors used,[5,19] or at a single point of relative humidity (γ was measured for NO_2 on TiO_2 and Saharan sand at RH = 25%).[18,23] However, γ has been found to show a strong dependence on humidity for some reactions. Both the increase and the decrease of γ have been observed as a function of RH.[7,22,24,25] Recently, it has been found that the heterogeneous uptake of NO_2 on soil[26] and montmorillonite[27] was lowered notably by water.

In a recent work,[16] the revised Community Multi-scale Air Quality Model (CMAQ), with simple heterogeneous chemistry, greatly minimized the gaps between the model and the observation results concerning inorganic components, while relatively large errors still remained. This means more refined kinetic parameters for the relevant reactions are required to further improve the model performance. In the real troposphere, RH typically varies from 20% to 90%. Thus, the quantitative dependence of γ on RH needs to be investigated case by case for these important heterogeneous reactions.[28] At the present date, reports on the RH dependent γ of NO_2 on kaolin and hematite are unavailable for modelling simulation.

The reactive process of NO_2 on dust is regarded as the adsorption and reaction of NO_2 with the surface oxides, followed by secondary processes, or the heterogeneous hydrolysis of NO_2 to yield HONO and HNO_3.[20] Besides surface nitrates and nitrites,[19,29–31] HONO is

State Key Joint Laboratory of Environment Simulation and Pollution Control, Research Center for Eco-Environmental Sciences, Chinese Academy of Sciences, Beijing, 100085, China. E-mail: honghe@rcees.ac.cn

† Electronic supplementary information (ESI) available: Diagram of the flow tube; evolution of NO concentrations with time during uptake of NO_2 on kaolin and hematite; a comparison of the uptake curves of NO_2 with or without the Na_2CO_3 denuder; the relative ratio of NO_2 removed by the Na_2CO_3 denuder to the initial NO_2 concentration at different RH values; linear mass dependence of the uptake capacity of NO_2 within 30 min on kaolin and hematite. See DOI: 10.1039/c5cp02223a

also detected as a gaseous product.[6,11,18] Under ultra-violet irradiation, the HONO yield (y_{HONO}) is 75%, 33% and 80% for reactions of NO_2 on pure TiO_2,[22] 1% TiO_2/SiO_2 and Saharan sand,[18] respectively. It has been postulated that the surface acidity, microstructure and other unknown factors control the production of HONO.[18] However, the HONO yields for heterogeneous reactions of NO_2 on kaolin and hematite are as yet unclear, and how the RH affects the HONO yield for the reactions of NO_2 on these materials is also unknown.

In this study, kaolin and hematite, which have been identified as common mineralogical components of dust samples,[32] were used as a proxy of mineral dust to investigate the effect of RH on the kinetics and HONO yields for reactions with NO_2. The uptake experiments were carried out at ambient RH and ambient pressure using a flow tube reactor. The quantitative dependence of uptake coefficients and HONO yields on RH on kaolin and hematite was obtained. The environmental implications were also discussed.

Experimental section

Materials

Hematite (AR) was obtained from Beijing Nanshang Chemicals Factory. Kaolin was supplied by Huaibei Junteng Kaolinite Co. Ltd and originated from Anhui province, China. The mineralogy was confirmed by X-ray diffraction (XRD) analysis (D/max-RB). The specific surface area of hematite and kaolin was 2.7 $m^2\ g^{-1}$ and 12.4 $m^2\ g^{-1}$, respectively, measured by nitrogen Brunauer–Emmett–Teller (BET) physisorption analysis (Quantachrome Autosorb-1-C). NO_2 standard gas (50 ppmv in N_2, Beijing Huayuan Gases Inc.), and high purity N_2 and O_2 (99.99%, Beijing AP BEIFEN Gases Inc.) were used as received.

Experimental methods

The experiments were performed in a 20 cm × 1.0 cm (i.d.) horizontal cylindrical coated-wall flow tube reactor in the dark (covered with aluminium foil) (Fig. S1, ESI†), which has been described in detail elsewhere[33] and is similar to that used by Ndour *et al.*[23] The temperature was maintained at 298 K by circulating water through the outer jacket of the flow tube reactor. Simulated air was used as the carrier gas, and the total flow introduced in the flow tube reactor was 770 ml min^{-1}, ensuring a laminar regime at ambient pressure. NO_2 was introduced into the flow tube through a movable injector with 0.3 cm radius. The NO_2 concentration was (150 ± 5) ppb and was measured using a NO_x analyzer (THERMO 42i), in which a molybdenum catalyst converts NO_2 to NO, which is subsequently measured *via* chemiluminescence, after which NO is oxidized by O_3. A Na_2CO_3 denuder tube (10 cm × 1.0 cm i.d.) was introduced between the exit of the flow tube reactor and the detector to trap the formed HONO, since it is also detected as NO_2 by the analyzer.[18] Thus, the HONO concentration was indirectly measured as the difference between the detected NO_2 signals with and without the Na_2CO_3 denuder in the sampling line. The collection efficiencies of the Na_2CO_3 denuder were measured to be 100% at different RH over 1 h for a 200 ppb HONO flow. A new denuder was installed before each uptake experiment to avoid the saturation effects with long exposure. This method has been verified in our previous work.[33] RH was adjusted by the ratio of dry N_2 to wet N_2 and measured using a hygrometer (Center 314). The powder samples were suspended in ethanol and dripped uniformly into the Pyrex flow tube, and dried overnight in an oven at 393 K. It has been confirmed that the adsorption of reactant gases onto the quartz tube is negligible in blank experiments.

The reaction kinetics, k_{obs}, was reported in terms of the uptake coefficient, which was proportional to the measured first-order rate constant derived from the uptake curves when the Na_2CO_3 denuder was used, according to the following equation,[18,33]

$$k_{obs} = \frac{\gamma_{obs}\langle c\rangle}{2r_{tube}} \quad (1)$$

where r_{tube}, γ_{obs} and $\langle c\rangle$ are the flow tube radius, the geometric uptake coefficient and the average molecular velocity of NO_2, respectively. The k_{obs} was determined by pulling the injector back to the end of the sample tube. Thus, the geometric inner surface area of the whole sample tube was used to calculate γ_{obs}. A correction for gas phase diffusion limitations was taken into account for γ_{obs} calculations using the Cooney–Kim–Davis (CKD) method.[34,35] Then, the true uptake coefficient (γ_t) was obtained from the mass dependence of γ_{obs} as follows,[25]

$$\gamma_t = [\text{slope}]\frac{A_g}{S_{BET}} \quad (2)$$

where [slope] is the slope of the plot of γ_{obs} *versus* the sample mass in the linear regime (mg^{-1}); A_g is the inner surface area of the sample tube (cm^2); and S_{BET} is the specific surface area of the particle sample ($cm^2\ mg^{-1}$).

Results and discussion

Fig. 1 shows the typical uptake curves of NO_2 on kaolin and hematite as well as the corresponding evolution of the γ_{obs} with time. The black and red lines show the data collected with 10 s and 1 min time resolution, respectively. As shown in Fig. 1A and B, once the kaolin or hematite sample was exposed to NO_2, a large initial NO_2 uptake was observed, followed by a quick recovery. After 20 min, a stable consumption of NO_2 was observed on both kaolin and hematite. The c/c_0 (20–30 min) was (0.869 ± 0.005) and (0.902 ± 0.006) for these two specific experiments, respectively. This steady uptake of NO_2 was always observed for all uptake experiments at different RH, which implies the occurrence of a catalytic reaction. When the samples were isolated from the reactant gas by moving the injector outside the reaction region, only a small amount of NO_2 (<4%) desorbed from both kaolin and hematite. This means that the reactive uptake should be the main contributor to the uptake of NO_2 on these samples.

Because NO is in thermodynamic equilibrium with NO_2, ~3% NO was always present in the reactant gas. Fig. S2 (ESI†)

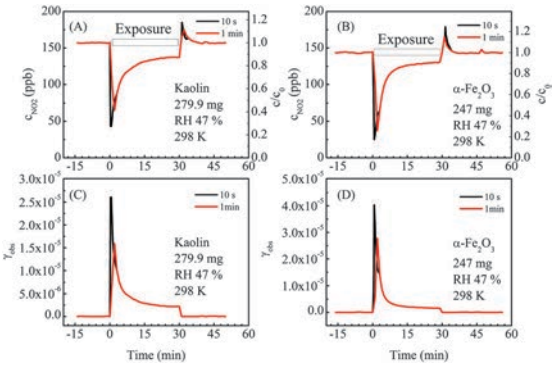

Fig. 1 Uptake curves of NO_2 on (A) 279.9 mg of kaolin and (B) 247 mg of hematite; and evolution of the observed uptake coefficient on (C) 279.9 mg of kaolin and (D) 247 mg of hematite at 298 K and 47% RH.

shows the evolution of NO concentrations with time during uptake of NO_2 on kaolin and hematite at a RH of 47% and 7%, respectively. Within the instrumental uncertainty, NO concentrations did not change during uptake experiments on hematite at all tested levels of relative humidity (7–74%). The uptake of NO on kaolin, however, was observed clearly at 7% RH, which suggests adsorption of NO onto kaolin. This phenomenon is opposite to that observed by Underwood *et al.*[19] using a Knudsen cell-mass spectrometer, in which NO was observed as the predominant gas phase product for the reaction of NO_2 with mineral oxides. This might result from different reaction conditions, such as mineral oxides, RH, concentration and pressure. In our work, the high concentration of O_2 (20%) should be favourable to the positive reaction in the equilibrium of NO and NO_2 when compared with the reaction taking place in the Knudsen cell reactor, at low O_2 pressure. On the other hand, RH in this study is much higher than that in Underwood's work.[19] A higher RH may be favourable to heterogeneous hydrolysis of NO_2. It should be pointed out that the variation of the NO concentration in the gas flow depends on the consumption and production of NO from both gas phase and surface reactions. The gas phase conversion from NO to NO_2 should have the same influence on the NO concentration regardless of the RH and the type of dust samples, because the initial NO and O_2 concentrations are the same. The surface reactions (5) and (6), which will be discussed below, can produce NO. Additionally, the gas phase reaction between HONO and NO_2[36] can also produce gaseous NO. Because higher HONO yields were observed at higher RH in this work, more NO might be formed at high RH from this reaction; subsequently, the uptake of NO was compensated at high RH on kaolin. On hematite, however, no difference was observed for NO uptake regardless of RH. This might be ascribed to reactions (5) and (6) being dominant even at a low RH or to the uptake of NO by hematite being negligible.

Using infrared spectroscopy, surface species including nitrates and nitrites have been well characterized for heterogeneous reactions of NO_2 on kaolin[6] and other mineral oxides.[19,29,30,37,38] The presence of surface nitrogen with oxidation states of +5, +4 and +3 was also confirmed using X-ray spectroscopy.[31] Additionally, gas phase HNO_3, NO, and HONO were detected.[6,19] Based on these previous studies,[19,30,39] the following reactions are summarized as the possible reaction pathways in the dark.

$$MO^- + NO_2(g) \rightleftharpoons MO\text{–}NO_2^-(ads) \quad (3)$$

$$MO + 2NO_2(ads) \rightleftharpoons MO\text{–}N_2O_4(ads) \rightleftharpoons MO\text{–}NO^+NO_3^-(ads) \quad (4)$$

$$MO\text{–}NO_2^-(ads) + NO_2(g) \rightarrow MO\text{–}NO_3^-(ads) + NO(g) \quad (5)$$

$$2MO\text{–}NO_2^-(ads) \rightarrow MO^- + MO\text{–}NO_3^-(ads) + NO(g) \quad (6)$$

$$M\text{–}O^- + NO_2(g) \rightarrow M\text{–}NO_3^-(ads) \quad (7)$$

$$2M\text{–}O^- + N_2O_4(ads) \rightarrow MO\text{–}NO_2^-(ads) + MO\text{–}NO_3^-(ads) \quad (8)$$

$$MONO_2^-(ads) + MO\text{–}H_2O(ads) \rightarrow MO\text{–}OH(ads) + MO^- + HONO(g) \quad (9)$$

$$M\text{–}OH + NO_2(g) \rightarrow M\text{–}O + HONO(g) \quad (10)$$

$$2NO_2(g) + MO\text{–}H_2O(ads) \rightarrow MO\text{–}HNO_3(ads) + HONO(g) \quad (11)$$

$$2M\text{–}OH + 2NO_2(g) \rightarrow MO\text{–}NO_3^-(ads) + MO\text{–}NO_2^-(ads) + MO\text{–}H_2O(ads) \quad (12)$$

MO in the above reactions refers to mineral oxide. The reactions (3), (5), (7), and (10)–(12) should contribute to the loss of NO_2 from the gas phase during uptake experiments. The reactions (5), (6), and (9)–(11) involving the release of gas phase NO and HONO should be responsible for the uptake of NO_2 at a steady state after the surface species are saturated. However, as shown in Fig. S2 (ESI†), the release of NO was not observed on either kaolin or hematite under all of the tested RH values (7–47%). This means that reactions (5) and (6) should follow a minor reaction pathway under our reaction conditions, although they cannot be ruled out yet owing to the possibility of adsorption or reactions in the gas phase or on the surface. Thus, the uptake at the steady state should mainly be related to the reactions involving HONO formation. The contribution of reactions (9)–(11) to NO_2 uptake and HONO formation will be discussed later.

Fig. 1C and D show the evolution of the γ_{obs} with reaction time. The γ_{obs} decreased quickly with reaction time due to the surface saturation by surface species as mentioned above. Thus, the time resolution had a great effect on the uptake coefficient. For example, in these two specific experiments shown in Fig. 1, the γ_{obs} (10 s) is 2.61×10^{-5} (279.9 mg kaolin) and 4.03×10^{-5} (247 mg hematite) at 298 K and 47% RH, while the corresponding γ_{obs} (1 min) is 1.59×10^{-5} and 2.78×10^{-5}, respectively. The γ_{obs} (SS) at the steady state (20–30 min) decreased to $(2.28 \pm 0.10) \times 10^{-6}$ and $(1.69 \pm 0.10) \times 10^{-6}$, respectively, with a decrease of one order of magnitude. Therefore, three values of γ_{obs} are reported here (γ_{obs} (10 s), γ_{obs} (1 min) and γ_{obs} (SS)).

As mentioned in the Experimental section, gas-phase diffusion was corrected for in γ_{obs} calculations using the

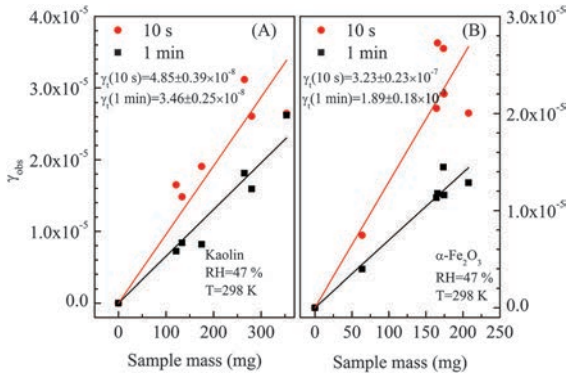

Fig. 2 Linear mass dependence for γ_{obs} on (A) kaolin and (B) hematite at 298 K and 47% RH.

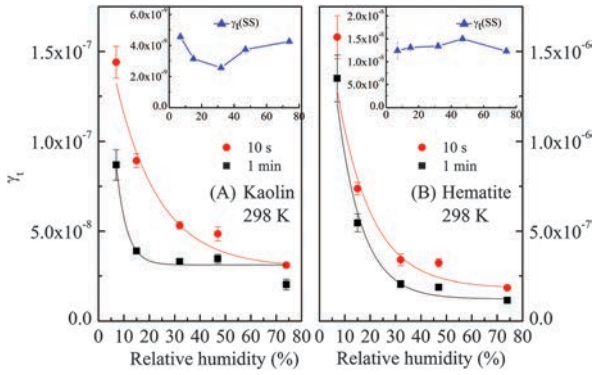

Fig. 3 Influence of RH on the γ_t of NO_2 on the surface of (A) kaolin and (B) hematite. The inset graph shows the corresponding γ_t (SS).

Cooney–Kim–Davis (CKD) method.[34,35] In the coated-wall flow tube reactor, powder samples with multilayer thickness were usually generated. In order to determine the probe depth of NO_2 in the multilayer samples, the response of γ_{obs} to the sample mass was measured. Fig. 2 shows the typical linear mass dependence of γ_{obs} on kaolin and hematite. Thus, the true uptake coefficient (γ_t, BET) can be obtained using eqn (2). The γ_t (10 s), γ_t (1 min) and γ_t (SS) of NO_2 on kaolin at 47% RH are $(4.85 \pm 0.39) \times 10^{-8}$, $(3.46 \pm 0.25) \times 10^{-8}$, and $(3.74 \pm 0.27) \times 10^{-9}$, respectively. The corresponding values are $(3.23 \pm 0.23) \times 10^{-7}$, $(1.89 \pm 0.18) \times 10^{-7}$, and $(1.50 \pm 0.05) \times 10^{-8}$, respectively, on hematite. The values of γ_t (10 s), γ_t (1 min) and γ_t (SS) at other levels of relative humidity are summarized in Table 1.

As shown in Table 1, both kaolin and hematite showed the largest γ_t of NO_2 at 7% RH. The γ_t (10 s) was $(1.44 \pm 0.10) \times 10^{-7}$ on kaolin, and it was $(1.58 \pm 0.13) \times 10^{-6}$ on hematite at 7% RH. Fig. 3 shows the influence of RH on the γ_t of NO_2 on the surface of kaolin and hematite. Assuming a Langmuir–Hinshelwood mechanism for the heterogeneous reaction of NO_2 on these samples and that the adsorption of water vapour can be described independently by a Langmuir isotherm with an equilibrium constant K_{H_2O}, the NO_2 surface coverage (θ_{NO_2}) under humid conditions is given by,[40,41]

$$\theta_{NO_2} = \frac{K_{NO_2}[NO_2]}{1+K_{NO_2}[NO_2] + K_{H_2O}[H_2O]} \quad (13)$$

where K_{NO_2} and K_{H_2O} are the Langmuir adsorption equilibrium constants for NO_2 and H_2O, respectively, and $[NO_2]$ and $[H_2O]$ are the concentrations of NO_2 and water vapor, respectively. The pseudo first-order rate coefficient of the NO_2 reaction follows

$$k_{1,NO_2} = \frac{k_{2,s}[SS]_s K_{NO_2}[NO_2]}{1 + K_{NO_2}[NO_2] + K_{H_2O}[H_2O]} \quad (14)$$

where $k_{2,s}$ is the second-order surface reaction rate constant and $[SS]_s$ is the adsorption site on the particle. By replacing eqn (14) with eqn (15) and (16),

$$\gamma = \frac{4k_{1,NO_2}}{A_S\langle c_{NO_2}\rangle} \quad (15)$$

$$[H_2O] = \frac{P^0_{H_2O}[RH]}{RT} \quad (16)$$

the influence of RH on the uptake coefficient can be described as

$$\gamma = \frac{4k_{2,s}[SS]_s K_{NO_2}[NO_2]}{A_S\langle c_{NO_2}\rangle + K_{NO_2}[NO_2]A_S\langle c_{NO_2}\rangle + \frac{P^0_{H_2O}[RH]K_{H_2O}A_S\langle c_{NO_2}\rangle}{RT}} \quad (17)$$

Because the uptake experiments were carried out at a constant NO_2 concentration, eqn (17) can be simplified as

$$\gamma = \frac{a}{b + c[RH]} \quad (18)$$

where $a = 4k_{2,s}[SS]_s K_{NO_2}$, $b = \langle c_{NO_2}\rangle + K_{NO_2}[NO_2]\langle c_{NO_2}\rangle$, and $c = \frac{P^0_{H_2O}K_{H_2O}\langle c_{NO_2}\rangle}{RT}$; A_S is the surface area of the particles;

Table 1 Summary of the measured NO_2 uptake coefficients (γ_t) and HONO yields (yHONO) for the heterogeneous reaction of NO_2 on kaolin and hematite at 298 K

	Kaolin				Hematite			
RH (%)	$\gamma_{t,ini}$ (10 s) ($\times 10^{-8}$)	$\gamma_{t,ini}$ (1 min) ($\times 10^{-8}$)	$\gamma_{t,ss}$ ($\times 10^{-9}$)	y_{HONO} (%)	$\gamma_{t,ini}$ (10 s) ($\times 10^{-7}$)	$\gamma_{t,ini}$ (1 min) ($\times 10^{-7}$)	$\gamma_{t,ss}$ ($\times 10^{-8}$)	y_{HONO} (%)
7	14.4 ± 0.01	8.69 ± 0.01	4.56 ± 0.15	3.4 ± 2.4	15.8 ± 1.30	13.5 ± 1.30	1.24 ± 0.18	19.4 ± 0.4
15	8.93 ± 0.39	3.89 ± 0.15	3.04 ± 0.16	9.0 ± 2.9	7.37 ± 0.35	5.46 ± 0.50	1.31 ± 0.07	39.1 ± 1.6
32	5.32 ± 0.21	3.30 ± 0.15	2.56 ± 0.01	18.0 ± 0.8	3.40 ± 0.33	2.06 ± 0.19	1.31 ± 0.06	72.1 ± 3.9
47	4.85 ± 0.39	3.46 ± 0.25	3.74 ± 0.27	41.0 ± 2.2	3.23 ± 0.23	1.89 ± 0.18	1.50 ± 0.05	78.2 ± 1.6
74	3.10 ± 0.14	2.03 ± 0.29	4.26 ± 0.06	49.4 ± 2.8	1.86 ± 0.07	1.16 ± 0.08	1.23 ± 0.06	77.4 ± 0.1

$\langle c_{NO_2} \rangle$ is the mean molecular velocity of NO_2; and $P^0_{H_2O}$ is the saturated vapor pressure of water at 298 K. As shown in Fig. S3 (ESI†), a Langmuir adsorption isotherm for water vapor and the Langmuir–Hinshelwood reaction mechanism for NO_2 on these particles can adequately describe the influence of RH on the uptake coefficient. The γ_t (10 s) decreased as RH increased. The resulting equations are,

on kaolin,

$$\gamma_t\,(10\text{ s}) = 4.47 \times 10^{39}/(1.75 \times 10^{46} + 1.93 \times 10^{45}[\text{RH}]) \quad (19)$$

on hematite,

$$\gamma_t\,(10\text{ s}) = 4.46 \times 10^{39}/(6.73 \times 10^{44} + 3.48 \times 10^{44}[\text{RH}]) \quad (20)$$

Thus, the γ_t (10 s) at a RH of 0% can be extrapolated from the above equations and are 2.55×10^{-7} and 6.63×10^{-6} on kaolin and hematite, respectively. The γ_t (10 s) values reported here fall within the reported ranges of γ_t, from $(8.1 \pm 0.2) \times 10^{-8}$ to $(2.3 \pm 0.4) \times 10^{-7}$ for NO_2 on kaolin,[6] and from 7×10^{-7} to 7.7×10^{-6} for NO_2 on hematite under dry conditions,[5,19] respectively. At high RH (32–74%), the average γ_t (10 s) of NO_2 on kaolin was $(4.42 \pm 1.17) \times 10^{-8}$, and it was $(2.83 \pm 0.84) \times 10^{-7}$ on hematite. It decreased by factors of ~3 and ~9 on kaolin and hematite, respectively, when compared with the γ_t (10 s) at 0% RH. The influence of water on the γ of NO_2 on hematite and kaolin is similar to that on soil,[26] while it is slightly different from that on montmorillonite.[27]

It has been well recognized that a higher concentration of the reactant gas should lead to a smaller initial uptake coefficient, owing to the surface saturation effect.[18] For the same reason and as illustrated in Fig. 1, a larger initial uptake coefficient should be obtained at a shorter exposure time. It should be pointed out that the reactors and reaction conditions in these studies related to NO_2 uptake are quite different. For example, Angelini *et al.*[6] measured the γ_t at 0% RH and at a NO_2 partial pressure from 2.3×10^{-4} to 3.6×10^{-3} mbar using a DRIFTS reaction chamber, and Underwood *et al.*[5,19] carried out their experiments at 0% RH and at a NO_2 partial pressure from 5.3×10^{-6} to 10^{-2} mbar using a Knudsen cell reactor. In our work, the NO_2 partial pressure was 1.6×10^{-4} mbar at ambient pressure, and the lowest RH investigated was 7%. The concentration of NO_2 in this work (1.6×10^{-4} mbar) was slightly lower than that used by Angelini *et al.*,[6] while it was higher than Underwood's.[5] Additionally, in DRIFTS experiments, the data collected within the first several minutes are usually used to calculate the uptake coefficients, whereas the time resolution of a Knudsen cell-mass spectrometer is often higher than 1 s. Thus, a lower time resolution should be achieved in Angelini's work,[6] while the time resolution was higher in Underwood's work.[5,19] Therefore, the γ_t (10 s) of NO_2 at 0% RH estimated in this work is larger than Angelini's results ($8.1 \pm 0.2 \times 10^{-8}$ at 2.3×10^{-4} mbar) on kaolin,[6] while it is smaller than that of Underwood's results (7.7×10^{-6} at 5.3×10^{-6} mbar) on hematite.[5]

As shown in Fig. 3, like the γ_t (10 s), the γ_t (1 min) of NO_2 also decreases with RH on kaolin and hematite. In particular, the curves in the low RH regions (<20%) are much steeper than those in the high RH regions. The decline of the initial γ with RH can be ascribed to competitive adsorption between H_2O and NO_2, similar to the competitive adsorption of O_3, NO_2 or COS with H_2O on mineral oxides.[22,24,25] It has been found that a monolayer of H_2O on kaolin is achieved at 13% RH,[6] and at 10% RH on hematite.[24] The initial γ of H_2O on mineral dust ($4.2 \pm 0.7 \times 10^{-2}$)[42] is much larger than that of NO_2, as discussed above. This means that adsorption of H_2O is preferred over NO_2 when the RH is lower than the RH of monolayer of water. This satisfactorily explains the quick decrease of the initial γ_t of NO_2 in the low RH range. In addition, the γ_t (1 min) is more sensitive to RH than that of γ_t (10 s) in the low RH range, because the longer exposure time is favourable to formation of a monolayer of water. However, as shown in the inset graphs in Fig. 3, the γ_t (SS) was not very sensitive to RH on hematite, while a decrease followed by an increase with RH was observed on kaolin.

HONO formation and HONO yields

Besides surface nitrites,[19,29,30,37,38] the presence of HONO(g) was qualitatively confirmed during the heterogeneous reaction of NO_2 on SiO_2[11] and kaolin[6] using UV spectroscopy. Using a Long Path Absorption Photometer (LOPAP)[20] or a NO_x analyzer,[18,22,23] the yields of HONO were also measured directly or indirectly for the photochemical reaction of NO_2 on TiO_2 and Saharan sand.[18,22,23] The formation of HONO can be explained by reactions (9)–(11). In fact, when reaction (3) and the dissociation reaction of H_2O to form the surface OH group are coupled with reactions (9) and (10), a catalytic cycle from NO_2(g) to HONO(g) can be realized by the reaction of the surface OH group as shown below. Thus, reactions (9)–(11) can be regarded as catalytic reactions.

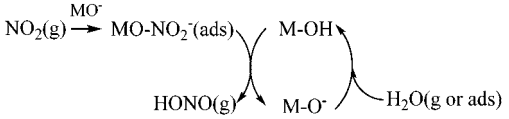

(21)

In the above experiments, a Na_2CO_3 denuder between the outlet of the reactor and the NO_x analyzer was used to trap the formed HONO. In order to investigate the HONO yields, uptake experiments without the Na_2CO_3 denuder were performed at 7–74% RH. Fig. S4 (ESI†) shows a comparison of the typical uptake curves of NO_2 on kaolin and hematite at 47% RH with or without the Na_2CO_3 denuder. As can be seen from this figure, the integrated uptake capacity (the total amount of NO_2 uptake by the sample within 30 min) for NO_2 with a Na_2CO_3 denuder was clearly larger than that without a Na_2CO_3 denuder on both kaolin and hematite. Thus, the difference between them represents the amount of HONO formed during the reaction. It should be pointed out that the Na_2CO_3 denuder can adsorb a small amount of NO_2 ($2.8 \pm 0.8\%$ regardless of RH, Fig. S5, ESI†). This difference might also partly result from the gaseous reaction between NO_2 and H_2O. However, in the experiments with a Na_2CO_3 denuder, adsorption of NO_2 or HONO from a gaseous reaction was saturated or subtracted before the

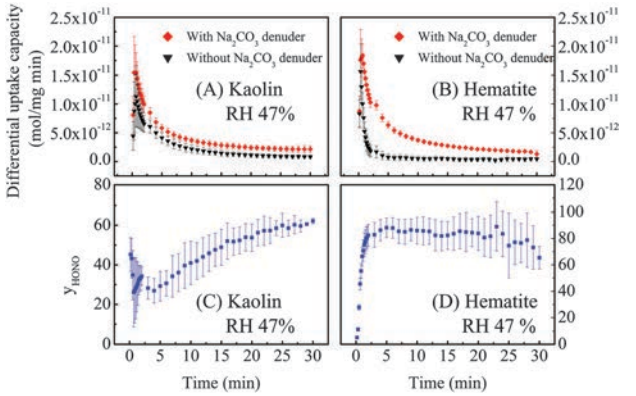

Fig. 4 Evolution of the (A) and (B) mass-normalized differential uptake capacity of NO_2, and (C) and (D) HONO yield with time.

samples were exposed to NO_2 gas. Therefore, the difference between uptake curves with and without the Na_2CO_3 denuder strongly supports the formation of HONO during the reactions of NO_2 on kaolin and hematite, and represents the net production of HONO from a heterogeneous reaction.

In the uptake experiments, uptake curves of NO_2 for different sample masses were independently measured. As discussed above, the integrated uptake capacity linearly depends on the sample mass over a wide mass range (Fig. S6, ESI†). Thus, by dividing the differential uptake capacity (the amount of NO_2 uptake by the sample within 1 min) by the sample mass, the normalized differential uptake capacity with or without a Na_2CO_3 denuder was obtained and is shown in Fig. 4. The error bars in Fig. 4A and B represent the standard deviation (σ) of 5–7 independent experiments. The averaged differential uptake capacity of NO_2 with a Na_2CO_3 denuder is clearly higher than that without a Na_2CO_3 denuder on both kaolin and hematite. Fig. 4C and D shows the evolution of HONO yield with reaction time. The error bars were calculated considering error propagation.

On kaolin, the initial y_{HONO} was around 30%, and then it gradually increased to 60%, while it increased quickly from 5% to 85% within 3 min on hematite. These results indicate that reactions (3), (5) and (7), which lead to surface nitrates and nitrites, mainly contribute to the initial uptake of NO_2 on either kaolin or hematite. This also satisfactorily explains the quick deactivation for uptake of NO_2 on kaolin and hematite (Fig. 1). However, at the steady state, the uptake of NO_2 should be mainly ascribed to reactions (9)–(11). Angelini *et al.*[6] proposed that reaction (9) might be related to HONO formation on kaolin because nitrites were not detected using both IR (at 1235 cm^{-1}) and ion chromatography. However, reactions (10) and (11) cannot be ruled out yet because a non-zero initial HONO yield was observed on kaolin (shown in Fig. 4C). In particular, the y_{HONO} on kaolin is around 50% at the steady state, which implies the importance of the disproportionation reaction (reaction (11)) in HONO formation on kaolin. On hematite, however, a very small initial y_{HONO} (5%) and a larger y_{HONO} at the steady state ($>50\%$) indicate that reactions (9) and (10) should be the main pathway for HONO formation. The accumulation of surface nitrites should explain the quick increase of y_{HONO} with time (Fig. 4D). Therefore, these results imply different mechanisms of HONO formation on different dust samples.

Fig. S6 (ESI†) shows the linear dependence of the integrated uptake capacity on the sample mass within 30 min. The slopes of these lines represent the integrated uptake capacity per unit sample mass. For example, at 47% RH, the slope was $(1.09 \pm 0.07) \times 10^{-10}$ mol mg^{-1} with a Na_2CO_3 denuder on kaolin, while it was $(6.40 \pm 0.19) \times 10^{-11}$ mol mg^{-1} when a Na_2CO_3 denuder was not used. For hematite, the corresponding slope was $(1.03 \pm 0.04) \times 10^{-10}$ mol mg^{-1} and $(2.25 \pm 0.24) \times 10^{-11}$ mol mg^{-1}. Therefore, using these values, the integrated HONO yield was calculated and summarized in Table 1. The influence of RH on the integrated uptake capacity and y_{HONO} is shown in Fig. 5.

As shown in Fig. 5, if a Na_2CO_3 denuder was not used, the integrated uptake capacity of both kaolin and hematite for NO_2 gradually decreased with RH within 30 min, whereas different responses of the integrated uptake capacity to RH were observed between these two minerals when a Na_2CO_3 denuder was used. On hematite, from 7% to 15% RH, the integrated uptake capacity decreased by about a factor of two owing to competitive adsorption and it did not change any more with a further increase in RH (dotted line). However, the integrated uptake capacity on kaolin decreased with RH from 7% to 32%, and then increased with a further increase in RH. This change trend was also observed for its γ_t (SS) as shown in Fig. 3. It should be noted that kaolin consists of neutral layers containing one octahedral aluminium hydroxide sheet bonded to one tetrahedral silicon oxide sheet through a plane of shared oxygen atoms.[6] Although kaolin has a low shrink-swell capacity compared to montmorillonite, it swells slightly with increased water adsorption,[43] which should make more reactive sites (M–O or M–OH) available. Thus, an increase of γ_t (SS) and the integrated uptake capacity was observed when the RH was higher than 32%. This is similar to the reaction of HNO_3 on Na–montmorillonite, on which the γ increases clearly at higher RH.[44] As shown in Fig. 5 and Table 1, the integrated HONO yield within 30 min increased from $(3.4 \pm 2.4)\%$ to $(49.4 \pm 2.8)\%$

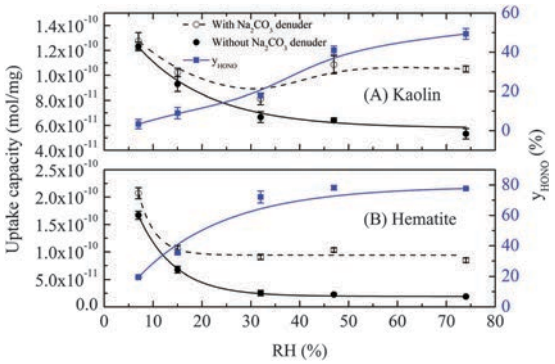

Fig. 5 Evolution of integrated uptake capacity and HONO yield within 30 min with RH on (A) kaolin and (B) hematite. The lines are guide to the eye.

on kaolin, and from (19.4 ± 0.4)% to (77.4 ± 0.1)% on hematite, when the RH increased from 7% to 74%. As discussed above, the values of the y_{HONO} also suggest that reaction (11) (disproportionation reaction with a HONO yield of 50%) should be the main mechanism for HONO formation on kaolin at high RH, while reactions (9) and (10) (with a HONO yield of 100%) should be important for HONO formation on hematite when the RH was larger than 32%.

It should be pointed out that HONO from the gas-phase reaction between NO_2 and H_2O at high RH might result in a positive bias for the measured heterogeneous HONO yields. However, this effect should be negligible in this study for the following reasons. Firstly, we measured the difference between the initial NO_2 concentrations with and without the Na_2CO_3 denuder at different RH values. If the gas phase reaction significantly contributes to the monitored HONO signal, the fraction of the removed HONO (measured as NO_2 and formed in the gas phase reaction) by the Na_2CO_3 denuder should positively respond to RH. However, as shown in Fig. S5 (ESI†), the relative ratio of NO_2 removed by the Na_2CO_3 denuder to the initial NO_2 concentration was constant (2.8 ± 0.8%), regardless of the RH value. Secondly, if gas phase reactions significantly contribute to the monitored HONO signal, a non-zero intercept should be expected when linearly fitting the uptake coefficient or the integrated uptake capacity to the sample mass at a fixed RH value, because the NO_2 converted to HONO in the gas phase should be a non-zero constant at the same residence time, NO_2 concentration and RH. However, as shown in Fig. 2 and Fig. S5 (ESI†), both the uptake coefficient and the integrated uptake capacity were linearly related to the sample mass with zero intercepts regardless of the RH values and sample types. Therefore, we are confident with the conclusion that the measured HONO yield was related to heterogeneous reactions on these samples.

Conclusions and atmospheric implications

Under dry conditions, the $\gamma_{t,ini}$ of NO_2 on kaolin and hematite was $2.55 \times 10^{-7}$and 6.63×10^{-6}, respectively. The values are comparable with those reported in the literature when the reaction conditions are taken into account.[5,6,19] However, the RH typically varies from 20% to 90% in the real troposphere. As found in this work, the $\gamma_{t,ini}$ decreased with RH. Therefore, the γ_t measured under dry conditions should overestimate the uptake ability of mineral dust toward NO_2. Using the measured $\gamma_{t,ini}$ in the RH range of 32–74%, we recommend that the $\gamma_{t,ini}$ of NO_2 on kaolin should be $(4.42 \pm 1.17) \times 10^{-8}$ at ambient RH, and $(2.83 \pm 0.84) \times 10^{-7}$ on hematite. These values are slightly larger than the values recommended by Crowley *et al.*[21] According to the model results, the $\gamma_{t,ini}$ should be greater than 10^{-4} to observe an appreciable impact on NO_x and O_3 concentrations for the interactions of NO_2 with mineral dust.[5] Thus, the small uptake coefficients measured at ambient RH in this work imply that heterogeneous reactions of NO_2 on mineral dust might be unimportant for NO_x and O_3 concentrations. At the present date, secondary inorganic aerosol (SIA) has attracted much attention for China's air pollution because SIA often abruptly increases during severe haze days.[15–17] The role of heterogeneous reaction in SIA formation has been confirmed in field measurements, laboratory and modelling studies. As the typical RH has often varied in the range of 40–80% in haze days in China,[15] the influence of RH dependent kinetics on particulate species formation needs to be evaluated with modelling studies in the future.

As a daytime source of OH radicals, HONO formation attracts much attention. In this work, the uptake of NO_2 at the steady state was found to be mainly related to HONO formation. Similar to the recommended $\gamma_{t,ini}$ at ambient RH, we also recommend the $\gamma_{t,ss}$ of NO_2 at ambient RH to be $(3.52 \pm 0.87) \times 10^{-9}$ and $(1.35 \pm 0.14) \times 10^{-8}$ on kaolin and hematite, respectively. The corresponding HONO yield is (36.0 ± 16.1)% and (75.9 ± 3.32)%. Thus, the uptake coefficient for HONO formation at the steady state ($\gamma_{t,ss,HONO}$) was calculated to be $(1.27 \pm 0.88) \times 10^{-9}$ and $(1.02 \pm 0.15) \times 10^{-8}$ on kaolin and hematite, respectively. Assuming the tropospheric concentration of NO_2 to be in the range from 10 ppb to 50 ppb[45] and that of mineral dust from 40 μm^2 cm^3 to 150 μm^2 cm^3 with a fraction of hematite of 6%,[13,46] the possible formation rate of HONO *via* the reaction of NO_2 on hematite in mineral dust varies from 4.8×10^4 to 9.0×10^5 molecules cm^3 per day using the estimated $\gamma_{t,ss,HONO}$ of hematite. Even if the $\gamma_{t,ss,HONO}$ of mineral dust is equal to that of hematite, the formation rate of HONO is estimated to be from 8.0×10^5 to 1.5×10^7 molecules cm^3 per day. This value is much lower than that on soot samples.[4] Therefore, the contribution of the heterogeneous reaction of NO_2 on mineral dust to tropospheric HONO might be negligible under typical atmospheric conditions. However, the mass loading of dust is often increased on severe haze days.[47] An *et al.*[48] found that heterogeneous reactions significantly enhance the concentrations of HONO and other particulate species in the North China Plain. This means that more comprehensive modelling studies based upon our kinetics should be carried out to fully evaluate the role of HONO formation from heterogeneous reactions on dust in regional air quality. It should be pointed out that the kinetic data were measured in the dark in this work, and other factors such as adsorbed HNO_3 have not been considered. It is necessary to investigate in the future whether irradiation has an enhancement effect on these reactions like that on Saharan sand[23] and whether the co-absorbed species, such as HNO_3, which were found to promote HONO decomposition on borosilicate glass surfaces,[49] have an influence on the HONO yield.

Acknowledgements

This research was financially supported by the Strategic Priority Research Program of the Chinese Academy of Sciences (XDB05010300) and the National Natural Science Foundation of China (51221892).

References

1 F. Arens, L. Gutzwiller, U. Baltensperger, H. W. Gaggeler and M. Ammann, *Environ. Sci. Technol.*, 2001, **35**, 2191–2199.
2 M. S. Salgado and M. J. Rossi, *Int. J. Chem. Kinet.*, 2002, **34**, 620–631.
3 J. McCabe and J. P. D. Abbatt, *J. Phys. Chem. C*, 2009, **113**, 2120–2127.
4 M. E. Monge, B. D'Anna, L. Mazri, A. Giroir-Fendler, M. Ammann, D. J. Donaldson and C. George, *Proc. Natl. Acad. Sci. U. S. A.*, 2010, **107**, 6605–6609.
5 G. M. Underwood, C. H. Song, M. Phadnis, G. R. Carmichael and V. H. Grassian, *J. Geophys. Res.: Atmos.*, 2001, **106**, 18055–18066.
6 M. M. Angelini, R. J. Garrard, S. J. Rosen and R. Z. Hinrichs, *J. Phys. Chem. A*, 2007, **111**, 3326–3335.
7 H. J. Li, T. Zhu, D. F. Zhao, Z. F. Zhang and Z. M. Chen, *Atmos. Chem. Phys.*, 2010, **10**, 463–474.
8 Y. Bedjanian and A. El Zein, *J. Phys. Chem. A*, 2012, **116**, 1758–1764.
9 R. Vogt and B. J. Finlayson-Pitts, *J. Phys. Chem.*, 1994, **98**, 3747–3755.
10 D. D. Weis and G. E. Ewing, *J. Phys. Chem. A*, 1999, **103**, 4865–4873.
11 A. L. Goodman, G. M. Underwood and V. H. Grassian, *J. Phys. Chem. A*, 1999, **103**, 7217–7223.
12 A. Indarto, *Res. Chem. Intermed.*, 2012, **38**, 1029–1041.
13 F. J. Dentener, G. R. Carmichael, Y. Zhang, J. Lelieveld and P. J. Crutzen, *J. Geophys. Res.*, 1996, **101**, 22869–22889.
14 Y. Zhang and G. Carmichael, *J. Appl. Meteorol.*, 1999, **38**, 353–366.
15 G. J. Zheng, F. K. Duan, H. Su, Y. L. Ma, Y. Cheng, B. Zheng, Q. Zhang, T. Huang, T. Kimoto, D. Chang, U. Pöschl, Y. F. Cheng and K. B. He, *Atmos. Chem. Phys.*, 2015, **15**, 2969–2983.
16 B. Zheng, Q. Zhang, Y. Zhang, K. B. He, K. Wang, G. J. Zheng, F. K. Duan, Y. L. Ma and T. Kimoto, *Atmos. Chem. Phys.*, 2015, **15**, 2031–2049.
17 H. He, Y. Wang, Q. Ma, J. Ma, B. Chu, D. Ji, G. Tang, C. Liu, H. Zhang and J. Hao, *Sci. Rep.*, 2014, **4**, 4172, DOI: 10.1038/srep04172.
18 M. Ndour, B. D'Anna, C. George, O. Ka, Y. Balkanski, J. Kleffmann, K. Stemmler and M. Ammann, *Geophys. Res. Lett.*, 2008, **35**, L05812, DOI: 10.01029/02007GL032006.
19 G. M. Underwood, T. M. Miller and V. H. Grassian, *J. Phys. Chem. A*, 1999, **103**, 6184–6190.
20 http://www.iupac-kinetic.ch.cam.ac.uk/.
21 J. N. Crowley, M. Ammann, R. A. Cox, R. G. Hynes, M. E. Jenkin, A. Mellouki, M. J. Rossi, J. Troe and T. J. Wallington, *Atmos. Chem. Phys.*, 2010, **10**, 9059–9223.
22 R. J. Gustafsson, A. Orlov, P. T. Griffiths, R. A. Cox and R. M. Lambert, *Chem. Commun.*, 2006, 3936–3938.
23 M. Ndour, M. Nicolas, B. D'Anna, O. Ka and C. George, *Phys. Chem. Chem. Phys.*, 2009, **11**, 1312–1319.
24 P. K. Mogili, P. D. Kleiber, M. A. Young and V. H. Grassian, *J. Phys. Chem. A*, 2006, **110**, 13799–13807.
25 Y. Liu, Q. Ma and H. He, *Atmos. Chem. Phys.*, 2009, **9**, 6273–6286.
26 L. Wang, W. Wang and M. Ge, *J. Environ. Sci.*, 2012, **24**, 1759–1766.
27 Z. Zhang, J. Shang, T. Zhu, H. Li, D. Zhao, Y. Liu and C. Ye, *J. Environ. Sci.*, 2012, **24**, 1753–1758.
28 C. E. Kolb, R. A. Cox, J. P. D. Abbatt, M. Ammann, E. J. Davis, D. J. Donaldson, B. C. Garrett, C. George, P. T. Griffiths, D. R. Hanson, M. Kulmala, G. McFiggans, U. Pöschl, I. Riipinen, M. J. Rossi, Y. Rudich, P. E. Wagner, P. M. Winkler, D. R. Worsnop and C. D. O. Dowd, *Atmos. Chem. Phys.*, 2010, **10**, 10561–10605.
29 Q. Ma, Y. Liu and H. He, *J. Phys. Chem. A*, 2008, **112**, 6630–6635.
30 C. Liu, Q. Ma, Y. Liu, J. Ma and H. He, *Phys. Chem. Chem. Phys.*, 2012, **14**, 1668–1676.
31 J. Baltrusaitis, P. M. Jayaweera and V. H. Grassian, *Phys. Chem. Chem. Phys.*, 2009, **11**, 8295–8305.
32 R. Wagner, T. Ajtai, K. Kandler, K. Lieke, C. Linke, T. Müller, M. Schnaiter and M. Vragel, *Atmos. Chem. Phys.*, 2012, **12**, 2491–2512.
33 C. Han, Y. Liu and H. He, *Environ. Sci. Technol.*, 2013, **47**, 3174–3181.
34 D. O. Cooney, S.-S. Kim and E. J. Davis, *Chem. Eng. Sci.*, 1974, **29**, 1731–1738.
35 D. M. Murphy and D. W. Fahey, *Anal. Chem.*, 1987, **59**, 2753–2759.
36 X. Lu, J. Park and M. C. Lin, *J. Phys. Chem. A*, 2000, **104**, 8730–8738.
37 V. H. Grassian, *Int. Rev. Phys. Chem.*, 2001, **20**, 467–548.
38 B. C. Hixson, J. W. Jordan, E. L. Wagner and H. M. Bevsek, *J. Phys. Chem. A*, 2011, **115**, 13364–13369.
39 C. R. Usher, A. E. Michel and V. H. Grassian, *Chem. Rev.*, 2003, **103**, 4883–4939.
40 U. Poschl, T. Letzel, C. Schauer and R. Niessner, *J. Phys. Chem. A*, 2001, **105**, 4029–4041.
41 M. Ammann, U. Poschl and Y. Rudich, *Phys. Chem. Chem. Phys.*, 2003, **5**, 351–356.
42 S. Seisel, Y. Lian, T. Keil, M. E. Trukhin and R. Zellner, *Phys. Chem. Chem. Phys.*, 2004, **6**, 1926–1932.
43 J. C. Miranda-Trevinol and C. A. Coles, *Appl. Clay Sci.*, 2003, **23**, 133–139.
44 C. D. Mashburn, E. K. Frinak and M. A. Tolbert, *J. Geophys. Res.*, 2006, **111**, D15213.
45 P. Wei, Z. Ren, F. Su, S. Cheng, P. Zhang and Q. Gao, *Acta Meteorol. Sin.*, 2011, **25**, 797–811.
46 Y. Liu, J. Ma and H. He, *Atmos. Chem. Phys.*, 2010, **10**, 10335–10344.
47 M. Tao, L. Chen, L. Su and J. Tao, *J. Geophys. Res.: Atmos.*, 2012, **117**, D12203, DOI: 10.1029/2012JD017915.
48 J. An, Y. Li, Y. Chen, J. Li, Y. Qu and Y. Tang, *Adv. Atmos. Sci.*, 2013, **30**, 57–66.
49 D. A. Syomin and B. J. Finlayson-Pitts, *Phys. Chem. Chem. Phys.*, 2003, **5**, 5236–5242.